JOURNAL OF MATERIALS SCIENCE 23 (1988) 1786–1804

Warm shock consolidation of IN 718 powder

S. L. WANG, M. A. MEYERS, A. SZECKET
Center for Explosives Technology Research and Department of Materials and Metallurgical Engineering, New Mexico Institute of Mining and Technology, Socorro, New Mexico 87801, USA

Explosive consolidation of the rapidly-solidified nickel-base superalloy powder IN 718 was successfully accomplished. The effects of explosive type, explosive-to-powder mass ratio, powder container material and thickness, type of confinement, shielding material, and pre-heating temperature were investigated. Conditions for satisfactory consolidation, with good mechanical properties and low microcrack density, were established. The best consolidation was achieved by using a double-tube design in which a flyer tube was explosively accelerated, impacting the (cylindrical) powder container. The powder was pre-heated at 525° C and the initial consolidation pressure was calculated to be 18 GPa, resulting in approximately 20% apparent interparticle melting (white-etching regions between particles). The quality of the consolidates was evaluated by optical and electron microscopy, and by tensile testing.

1. Introduction

Shock consolidation is accomplished through the propagation of a shock wave through the powder; this shock wave generates a number of high-pressure and/or high-strain-rate events that may produce the consolidation of the powder [1]. In metals, powder-to-powder impact with jetting and rapid localized deformation, high pressures between the particles, and particle-to-particle friction are the principal mechanisms by which bonding is achieved [2–9].

Considerable research effort has been devoted to consolidating rapidly-solidified (amorphous and crystalline) metal powders, but cracking remains a major problem. Rapidly-solidified superalloys have been successfully consolidated either by explosives [10–12] or by gas-gun techniques [13]. Interparticle bonding has been attributed to the formation of an interparticle melting layer. Recent experiments by Vreeland *et al.* [14] have identified an amorphous phase in these "interparticle melt" regions in shock-consolidated microcrystalline Markomet 1064. Thus, the interparticle regions presenting unique etching characteristics can be considered as molten and resolidified material. In spite of the fact that Meyers *et al.* [10], Morris [5], Prummer [15], Meyers and Pak [11], Wang *et al.* [12], and Thadhani and Vreeland [13] demonstrated that nickel-base superalloy powders could be successfully consolidated, specimens of appreciable dimensions have not yet been produced. In the gas-gun experiments [13], this is ascribed to the limiting gun bore diameter; in explosive fixtures, this is due to excessive cracking.

The objectives of the investigation whose results are presented herein were to (a) consolidate specimens of a dimension sufficient for tensile testing, (b) eliminate, as much as possible, cracks from the compacts, and (c) characterize the mechanical and microstructural features of shock-consolidated superalloy. In order to accomplish this, a number of experimental configurations providing different stress pulses were attempted. IN 718 powder prepared by the rotating electrode process (REP) by Amdry Alloy Metals Inc. was used in this investigation. The powder particles are shown in Fig. 1. In Fig. 1a one can see that there are numerous satellite particles present. Fig. 1b shows the etched cross-section of a particle; the structure is microdendritic. The dendritic arm spacing for the Inconel 718 alloy powder was equal to approximately 2 μm. All particles were between meshes 170 and 200, which correspond to sieve openings between 74 and 88 μm. The dendritic arm spacing is directly related to the mean cooling rate undergone by the particles. According to Morris [4] this corresponds to a cooling rate of 10^5 K sec^{-1}; this value is typical of REP.

2. Experimental techniques

43 compaction experiments using the cylindrical geometry were conducted in this investigation, and a number of different set-ups were introduped. An earlier investigation on RSR Mar M-200 [10, 11] yielded successful compacts with excellent hardness, interparticle bonding, compressive strength (on small-scale specimens) but profuse cracking. Explosives with high detonation velocities had previously been used. In an effort to minimize cracking, explosives with lower detonation velocities were introduced. Cracking was eliminated, but consolidation was poor. Parameters that were varied were detonation velocity, amount of explosive, material of the central mandrel, confinement of explosive and shielding layer between explosive and metal powder container. These attempts are described in detail by Wang [16]. Parallel experiments conducted with the Sandia calibrated fixtures showed that pressure is a parameter of foremost importance in consolidation [12]. A material parameter of great importance is the powder porosity (or distention). This porosity has a great effect on the energy deposited at the powder surfaces by the shock compression pulse.

0022–2461/88 $03.00 + .12

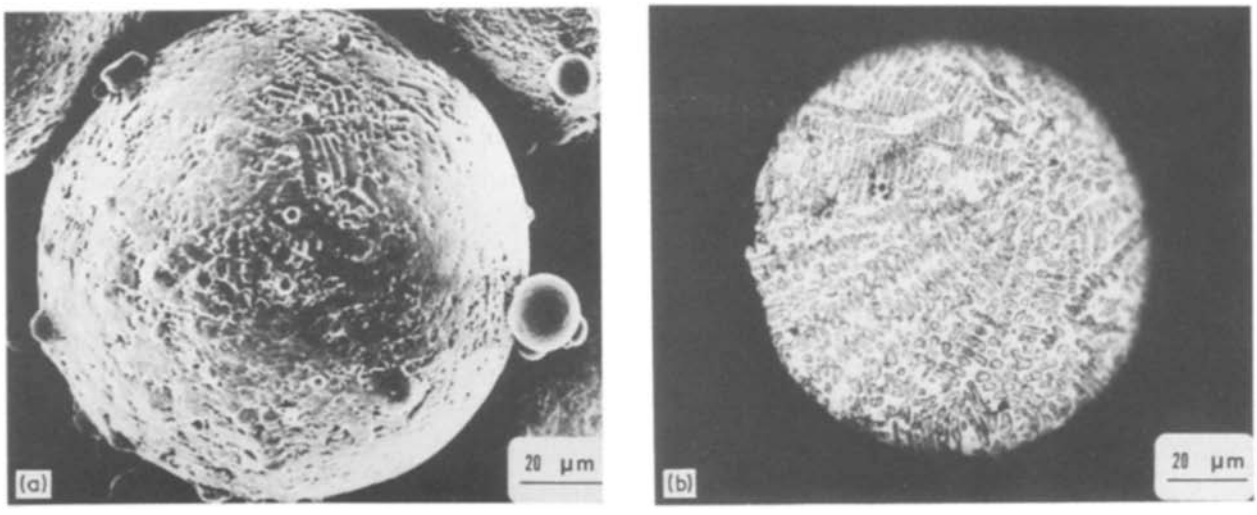

Figure 1 REP Inconel 718 powder produced by Amdry Alloy Metals Inc.: (a) scanning electron micrograph, (b) optical micrograph of particle cross-section.

The development of the double-tube implosion technique, in the cylindrical geometry, resulted in considerable improvement in the quality of the compacts; this technique is described separately [17]. The best consolidates were obtained by pre-heating the compacts. For this, the fixtures had to be modified. The powder was packed in a steel tube container and sealed at a 10^{-5} torr vacuum in order to minimize the oxidation during the pre-heating period. The powder was pre-heated from 600 to 850° C and then removed from the furnace and made to slide down to the assembly by the fixture shown in Fig. 2. The time interval between removal of the powder container from the furnace and detonation was recorded. From

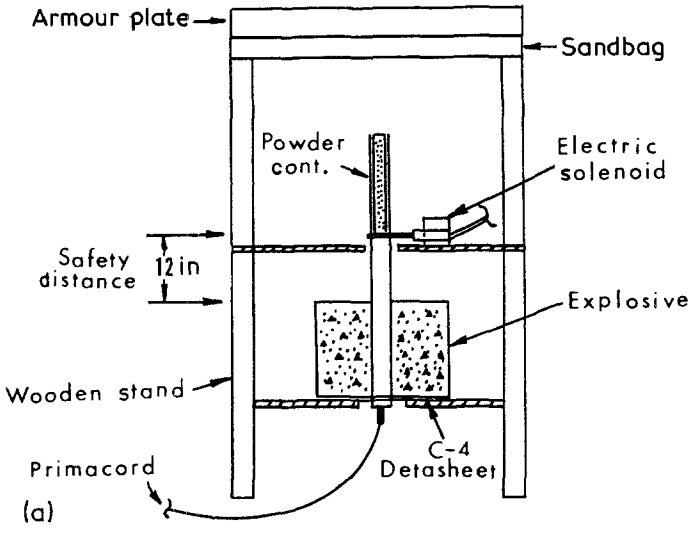

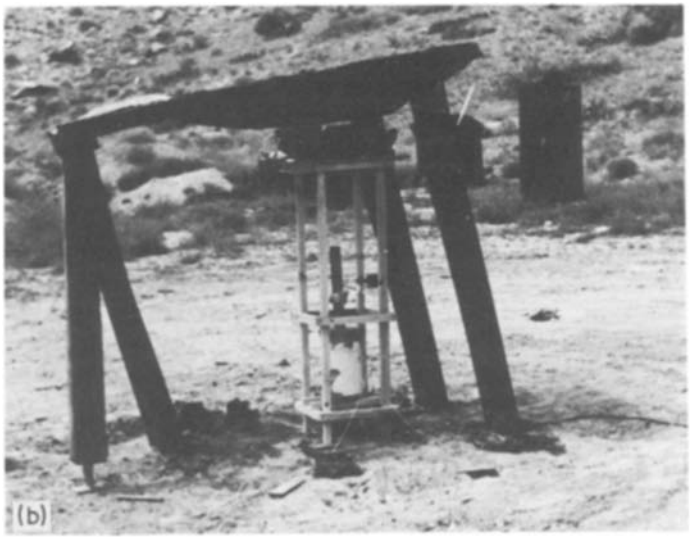

Figure 2 (a, b) Experimental set-up for powder compaction of pre-heated containers. 12 in. = 305 mm.

this cooling time, one can infer the pre-heating temperature at the detonation point by a temperature–time calibration curve. The powder container was allowed to drop into the assembly by activating a solenoid switch from a safe area. The time from removing the container from furnace to activation of the solenoid was less than 2 min. Immediately upon activation of the solenoid switch the system was fired. Initiation was at the bottom of the system. The armour plate in the top of the fixture was designed for easy recovery of the specimen. A sandbag was placed under the armour plate to prevent the specimen from being damaged by direct collision with the steel plate.

The techniques used for characterizing the compacts were optical and electron microscopy, and mechanical testing. These techniques are briefly described below.

The structures of the compacted specimens were studied first by visual inspection, and then by optical microscopy. Each compacted specimen was sectioned at equally spaced intervals, depending on the length of the container remaining at the explosion. These cross-sections were then mechanically polished through 0.06 μm alumina, and etched in Marble's reagent for 30 to 60 sec. Scanning and transmission electron microscopy were further used to observe the interparticle melting and bonding as well as the fracture morphology. Thin foils were prepared from selected areas by mechanically thinning down the specimens to a thickness of approximately 0.15 mm. Discs, 3 mm in diameter, were punched and electrolytically polished in a Fishione jet thinner. A 20% perchloric acid in methanol solution was used at 25 V and 20 mA and at a temperature of about $-20°$ C.

Quantitative metallography was performed on selected compacts to determine the pore fraction and the volume fraction of the interparticle melting zone. The pore and interparticle melting fraction was determined using the point-counting technique. This technique used a transparent grid of lines spaced 2 mm superimposed on a photomicrograph; the fraction of points falling on the pore or melting zone (the latter etches white and surrounds otherwise unaltered powder particles), as compared to the total number of points, was counted.

Microhardness measurements were made across the diameter of explosively compacted samples using a Leco microhardness tester at a load of 100 g. Microhardness of uncompacted powders was also measured by mounting and polishing.

Tensile tests were performed in the post-explosionem condition and after ageing. Tensile tests at ambient temperature were performed in an Instron 1122 testing machine at a strain rate of 10^{-4} sec^{-1}, according to ASTM Standard E-151; tensile specimens were cut in thin sheets in the transverse cross-section and had gauge dimensions of 21 mm $\times$ 2 mm $\times$ 0.5 mm. Tensile tests were also conducted at General Electric Aircraft Engine Division (Cincinnati, Ohio) at ambient and high temperatures. These specimens were cylindrical with threaded ends. Their diameter (in the reduced section) was 3.15 mm; the gauge length was 16.5 mm, and overall length was 37 mm. They were machined so that their axis was parallel to the compacted cylinder axis. The ends were shot-peened in order to decrease the tendency for fracture initiation at the threads.

3. Results and discussion

3.1. Stress-wave profile

There is considerable controversy in the literature regarding the critical parameters for shock consolidation, and exploratory experiments were devised to vary, as much as possible, the shape of the shock pulse. These experiments were coupled with calibrated shock consolidation experiments using Graham's Sandia fixtures [12]. Although the composition of the powder used in the Sandia fixtures is slightly different (IN 100) the results correlated well with those of the cylindrical fixtures. In these calibrated experiments, the following parameters could be varied, in a quantitative and reproducible way:

(a) peak pressure,
(b) pulse duration,
(c) average temperature.

While peak pressure and pulse duration are discussed in the literature, it was surprising to realize that the shock temperature played a vital role. The importance of the temperature (equilibrium bulk temperature) is in accord with the theories of Gourdin [6, 7] and Schwarz *et al.* [8]. The results of this investigation are described elsewhere [12] and the main conclusions were:

(i) The mean pressure for strong bonding, with approximately 10% interparticle melting, is about 20 GPa. The pressure required for bonding is dependent on porosity, as is discussed in detail by Meyers and Wang [17].

(ii) The pulse duration seems to play a role in the consolidation. However, the fraction of interparticle melting regions does not increase with pulse duration, in the 2.5 to 9.8 μsec range.

(iii) The shock temperature is an important parameter. It significantly enhances interparticle melting. At identical pressures and pulse durations, the regions undergoing the highest temperatures exhibit the greatest amount of (apparent) interparticle melting.

The effect of temperature can be qualitatively described by Fig. 3. In a shock front, the energy irreversibly dissipated is ΔE_1, (Fig. 3a). If the pressure reaches its maximum after the material has been densified by a lower stress wave, the temperature is much lower. In a shock front, the jump conditions establish the irreversible work, most of which manifests itself as a temperature increase; a small fraction is stored as defects in the material. A gradual increase in pressure on the other hand, allows densification at lower pressures, with less energy release. If the high-pressure pulse travels in a material that is already densified, the residual temperature increase is much less significant.

3.2. Exploratory experiments with cylindrical geometry

Earlier work by Meyers *et al.* [10] and Meyers and Pak

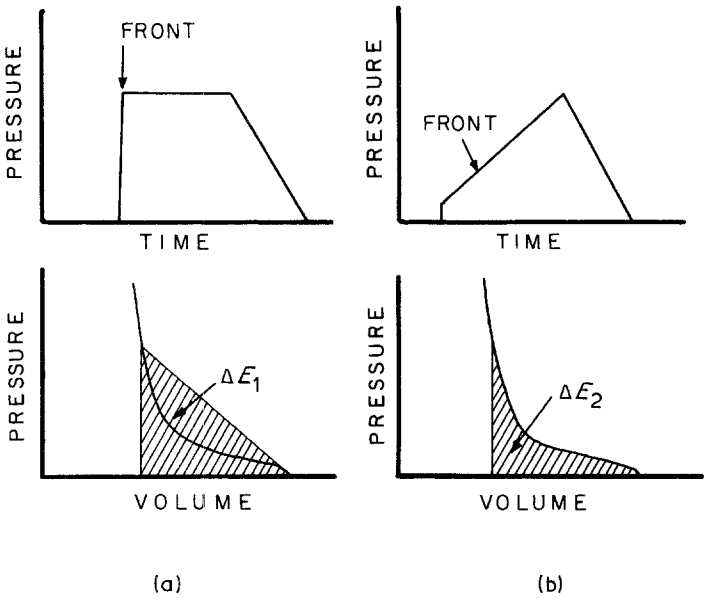

Figure 3 Irreversible energies (heat) ΔE_1 and ΔE_2, for different stress-wave configurations: (a) rapidly rising stress, (b) slowly rising stress.

[11] showed that the nickel-base superalloy Mar-M200 could be successfully consolidated by explosively-generated shock waves. Nevertheless, these experiments failed to yield specimens sufficiently large for the preparation of tensile specimens. In these experiments, high-detonation-velocity explosives were used, and extensive cracking of the specimens was associated with consolidation. In order to overcome this problem, approximately 40 experiments were conducted in this investigation in order to determine the effects of a number of parameters on shock consolidation. The details of assemblies and results are described in greater detail by Wang [16]. In all experiments, explosives with a lower detonation velocity (ANFO and ANFO-TNT mixtures) were used, in order to minimize cracking.

The first series of experiments using the cylindrical geometry was conducted with the single-tube set-up. In order to increase the detonation velocity, TNT was added to ANFO. At a constant explosive/powder weight ratio and detonation velocities increasing from 3000 to 5000 m sec^{-1}, no strong consolidation could be observed. In the second series, the explosive/powder weight ratio was increased at a constant explosive composition (ANFO). The effect of this is to increase the duration of the shock pulse, at a constant pressure. Again, although full densification was achieved, little interparticle melting was observed. In the third series, the cylindrical powder container wall thickness was varied. An increase in the container wall thickness resulted in an improvement in the quality of consolidation. The confinement of the explosive charge was investigated in Series 4. The explosive charge was encased in polyvinyl chloride (PVC), steel, or concrete. There were no noticeable positive effects of confinement. In the fifth series, a shielding material was placed between the explosive and the powder container tube in order to alter the shock front configuration. Wood, sand and lead were used with no significant effect. At the low detonation velocities used, total densification was always achieved, but the integrity of the compacts was low. The sixth series of experiments used the double-tube (or flyer-tube) technique. This technique resulted in improved consolidation at low detonation velocities, and is described in detail in a separate paper [17]. In order to further decrease cracking of the specimens, high-temperature experiments utilizing the flyer-tube technique were performed. The results are described in Section 3.3.

3.3. Hot-consolidation experiments

A total of nine tests, divided in three groups, were conducted using different explosives in order to vary the pressure and pre-heating temperature. The powder container and flyer-tube dimensions and materials were kept constant. The initial pressures generated by this technique were calculated according to the procedure described in a separate paper [17].

3.3.1. Optical metallography

Fig. 4 shows the metallographs of Experiment 39, which was compacted at the pre-heating temperature of 740° C. The other warm-consolidation experiments yielded specimens with similar characteristics. Fig. 4a shows the polished surface; generally, voids can be seen in most compacts with different degrees. Figs 4b, c and d show the specimen surface after etching. Profuse white regions are observed. These white regions are attributed to melting by several investigators. It is also possible that the formation of these voids is due to the entrapped air, which exists inside the powder container due to improper evacuation. These voids could have a very deleterious effect on the low-cycle fatigue life of the superalloy, since they can act as nucleation sites for cracks. The interparticle melting percentages are listed in Table I. The quality of the consolidates is directly related to the amount of interparticle melting. They vary between 9.5 and 31.8%; these values are significantly higher than those of specimens from Tests 1 to 32. By comparing the interparticle melting percentages in Tests 33 (room temperature) and 38 (580° C), conducted at approximately the same initial pressure (15 GPa), it can be seen that

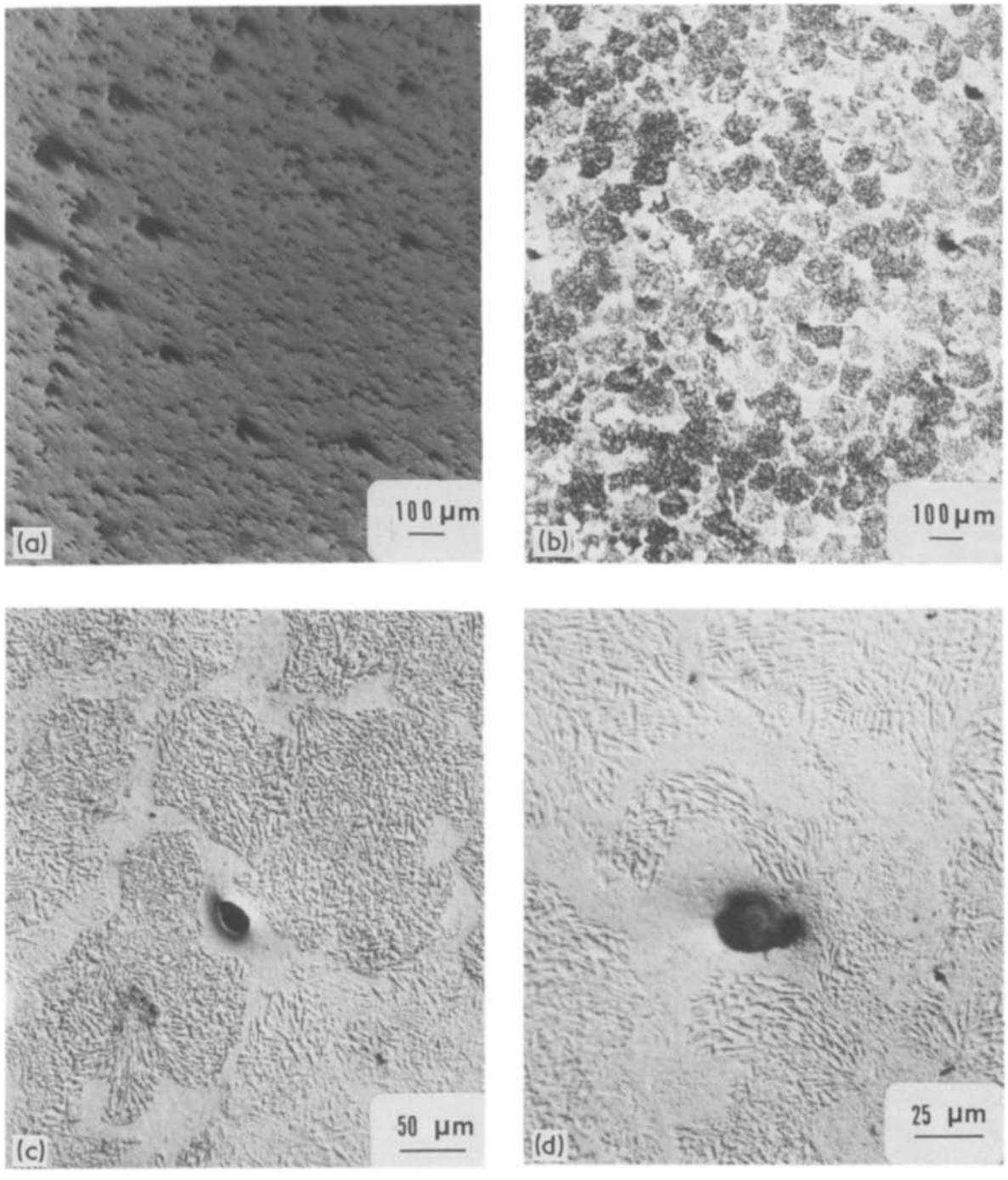

Figure 4 Optical metallographs of specimen pre-heated to 740° C and consolidated at a pressure of 18 GPa: (a) polished surface; (b, c, d) etched surface at different magnifications.

the temperature has a definite effect. The interparticle melting percentage in Test 38 is triple that of Test 33. Energy-dispersive X-ray analysis (EDX) was employed to make a chemical analysis of the composition in the interparticle melting zone and in the particle interior. X-ray spectra (Fig. 5) indicate that the chemical composition is fairly uniform. This illustrates that no segregation occurred during interparticle melting and resolidification.

An upper bound for the fraction of melted material can be calculated from the simple equation presented by Schwarz *et al.* [8]:

$$L = \frac{P_1 V_0 (m - 1)}{2[C_p(T_m - T_0) + H_m]}$$

The numerator of this equation is a simplified estimate of twice the energy deposited in the powder by the shock pulse, while the denominator is the energy absorbed in melting the material. The values for IN 718 were obtained by weight-averaging for the three principal constituent elements: nickel, iron, and chromium. The weight fractions were assumed to be 0.637, 0.178, and 0.185, respectively. This provided a heat capacity, C_p, of 581 J K kg^{-1}, a heat of fusion, H_m, of 258 kJ kg^{-1}, and a melting point, T_m, of 1826 K. The specific volume, V_0, was taken as 0.121 cm^3 g^{-1} and the distention, m, was equal to 1.67 (40% porosity). T_0 is the initial temperature and P_1 is the shock pressure. The calculated and measured melting fractions are shown in Fig. 6. Although they

TABLE 1 Experimental results for high-temperature consolidation experiments

Test No.	Calculated pressure (GPa)	Pre-heating temperature (°C)	Consolidate properties			
			0.2% YS (MPa)	UTS (MPa)	Hardness (HV100)	Measured interparticle melting (%)
31	3	R.T.*			470	2.1
32	8	R.T.			487	3.1
33	15	R.T.	534	761	496	6.5
41	3	525		423	440	9.5
43	8	525	877	1165	328	19.1
			(aged)1034	1210	429	
34	8	580	560	566	485	10.5
38	15	580	545	757	344	24.3
			(aged) 799	1146	421	
37	18	580	598	788	348	25
40	8	740	507	689	344	15.1
36	15	740	540	787	316	27.3
39	18	740	683	855	320	31.8
			(aged) 901	1239	421	

*Room temperature.

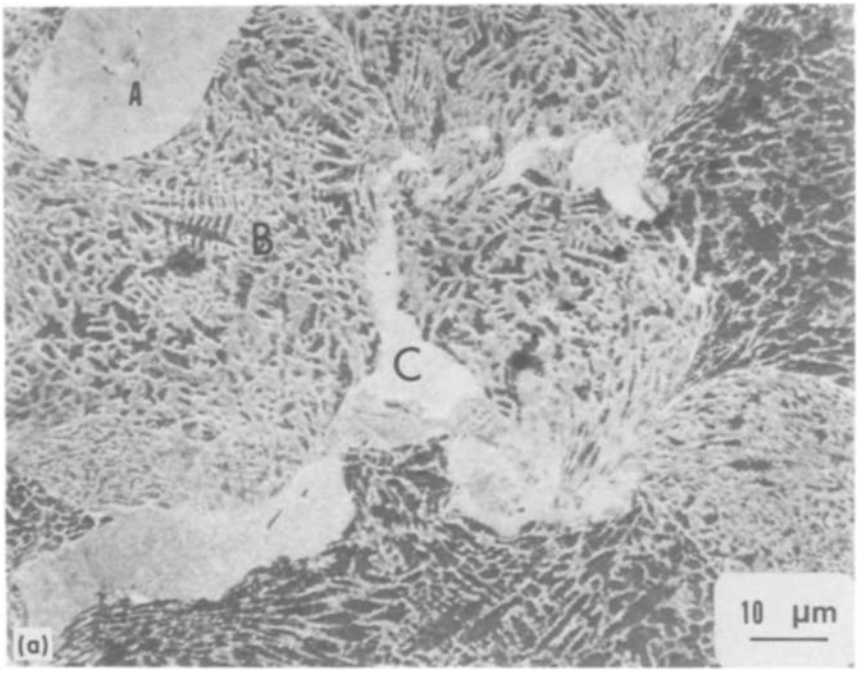

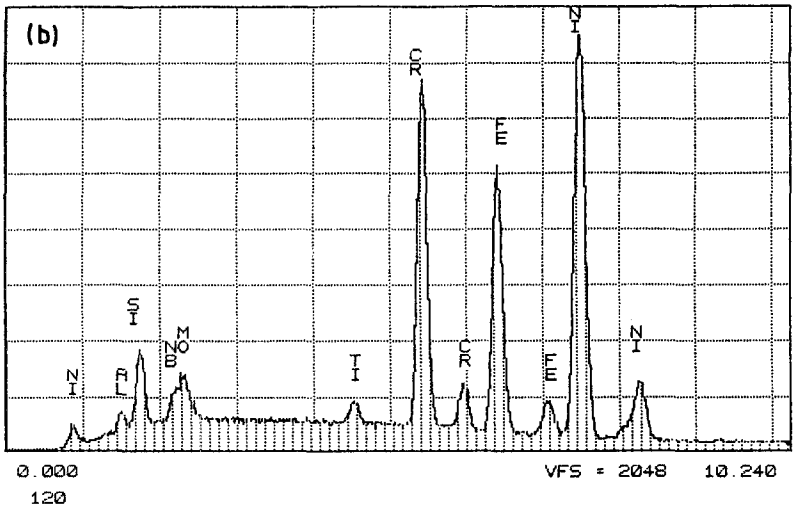

Figure 5 EDX analysis of compact (Specimen 43, aged): (a) SEM of etched surface, (b) X-ray spectrum of Point A, (c) X-ray spectrum of Point B, (d) X-ray spectrum of Point C.

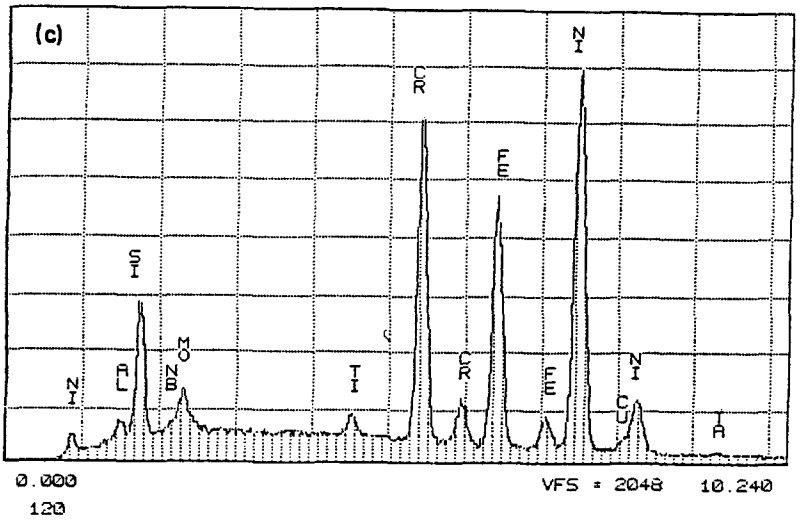

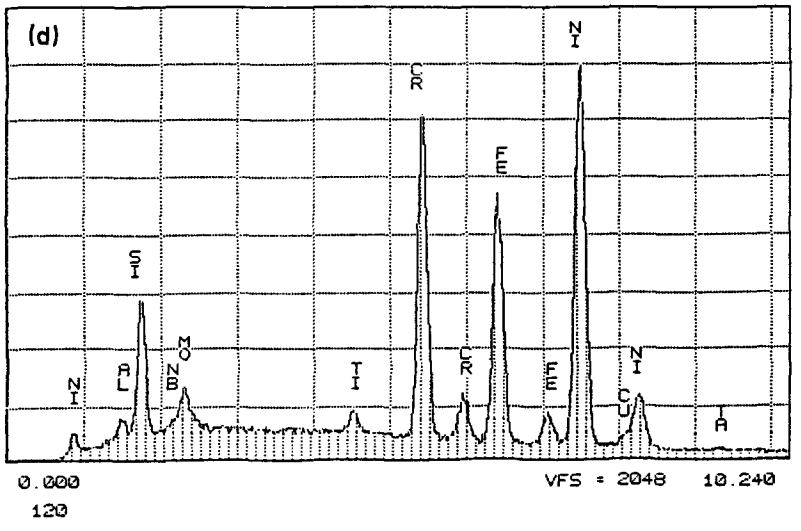

Figure 5 Continued.

are substantially different, two qualitative observations can be made:

(a) The melting fraction, at a constant pressure, increases with consolidation temperature. Thus, hot consolidation is an effective means of enhancing bonding without recourse to increasing pressure.

(b) The melting fraction increases as pressure increases.

The considerable discrepancy between calculated and measured melting fractions has several causes: (i) Schwarz *et al.* [8] assume that the temperature of the melt pool does not exceed the melting point; (ii) material strength is not considered and regions being plastically deformed undergo considerable heating without melting; thus, energy is not all consumed by melting regions. Indeed, Vreeland *et al.* [14] modified the earlier model of Schwarz *et al.* [8] by assuming that part of the energy went to the centre of the powders and obtained a much better correlation with experimental results. The two effects above would produce a reduction in the calculated melting fraction.

An additional feature of the measured melting fractions, not predicted by the simple model of Schwarz *et al.* [8], is that they seem to reach saturation levels. This can be qualitatively explained by the molten material being formed as the voids are filled. Thus, for a distention of 0.67 (40% porosity) the material that will flow and melt is determined by the geometry of the collapse process.

3.3.2. Mechanical properties

The results of mechanical tests are also listed in Table I including yield strength (0.2% offset), ultimate tensile strength and microhardness. Two tensile tests were conducted for each condition. The tensile properties were obtained with the same transverse specimens. The yield strength of Test 33, conducted at ambient temperature using the double-tube configuration, is equal to 534 MPa. The superior yield strength in shock-consolidated specimens is due to shock-hardening of the material.

The stress–strain curve of Compact 33 is typical of f c c materials, with work-hardening after yielding; the maximum strength is equal to 761 MPa. Fracture immediately followed the maximum tensile stress. No yield strengths could be obtained for single-tube (Test 31) and double-tube small-gap (Test 32) compaction because the compacts were broken during tensile specimen preparation.

The compact having the highest yield stress is Test 43, in which the container was pre-heated to 525° C and consolidated at 8 GPa; the resultant yield stress was 877 MPa. Another good consolidation resulted from Test 39, with a yield strength of the order of 683 MPa. It is interesting that in Test 39 the

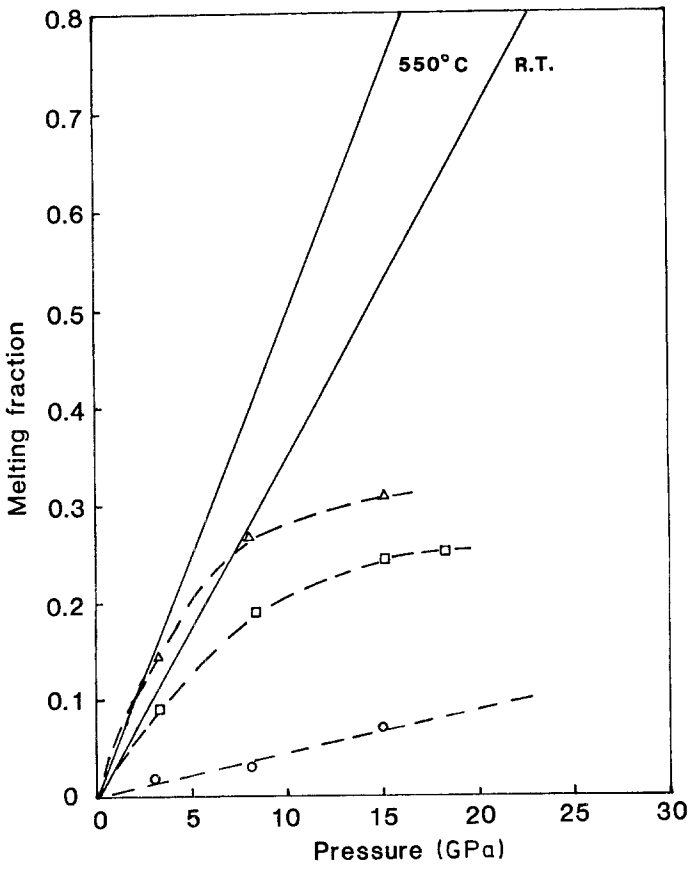

Figure 6 (——) Calculated and (– – –) measured melting fractions as a function of pressure for room- and high-temperature compactions: (○) room temperature, (□) 525 to 580° C, (△) 740° C.

pressure, pre-heating temperature, and fraction of interparticle melting all are higher than in Test 43 but the yield strength is lower than that of Test 43. This could be due to large interparticle melting pools containing many voids. These large interparticle melting pools are the weak points and lead to fracture during tensile testing.

The effect of pre-heating temperature on the yield strength can be seen by comparing Tests 33, 38 and 36, which were conducted at the same pressure level of 18 GPa (see Table I). The yield strengths of these compacts are in the same range, although the pre-heating temperatures are somewhat different. This indicates that the pre-heating temperature is not a critical parameter for consolidation. The main beneficial effect of pre-heating is in softening the powder, allowing it to flow and decreasing cracking. Linse [18] described the effect of elevating the powder temperature in dynamic compaction by the pressure against specific volume Hugoniot path. The powder is softened as the temperature is elevated and densified at lower pressure levels. The Hugoniot curve is then brought closer to the lower pressure levels. This also indicates that the higher pre-heating temperature regimes require less energy for compaction.

Microhardness data are also included in Table I. Cold compacts have a higher hardness than pre-heated compacts. The hardnesses of cold compacts exceed $H_v = 470$ while in most pre-heated compacts, the hardness is in the order range $H_v = 300$ to 400. This is consistent with the tensile results. Fig. 7 shows the variation of microhardness across the radius of the cross-section for selected samples. Microhardnesses are uniformly distributed from the centre to the outer rim. This indicates that the shock pressure is uniform in these specimens. The dense deformation substructure increased the microhardness of the particle from $H_v = 230$ in the as-received condition to $H_v = 500$ in the cold-consolidation condition. The strengthening effect due to shock waves is well known. The microhardness for the shock-consolidated and aged samples (Test 39) is approximately $H_v = 420$. This value indicates that precipitation-hardening is not as effective a strengthening mechanism as work-hardening. The warm compactions give the lowest hardnesses of compacts, and the reduction in hardness is believed to be due to recovery and/or recrystallization.

The pre-heating temperature may also have contributed to the amount of interparticle melting. Generally, the more the interparticle melting, the better the consolidation and the higher the strength that can be obtained. Fig. 8 shows a plot of strength against fraction of interparticle melting. The yield and ultimate tensile strengths increase with increase of interparticle melting fraction. Fig. 8 shows that the yield strength of the specimens compacted at 580° C is higher than for specimens compacted at 740° C. This can be understood by the fact that high temperature results in greater recovery or recrystallization of the microstructure than low temperature. This will be discussed again in Section 3.3.4. The pressure increase results in interparticle melting and yields strength increases at each pre-heating temperature. This is easy to understand from a total input energy aspect. The greater the energy input, the higher the localized temperature and the greater the interparticle melting.

Since nickel-base superalloys derive a substantial portion of their strength from precipitation, it was thought that the combination of shock-wave strengthening and ageing would lead to an even higher

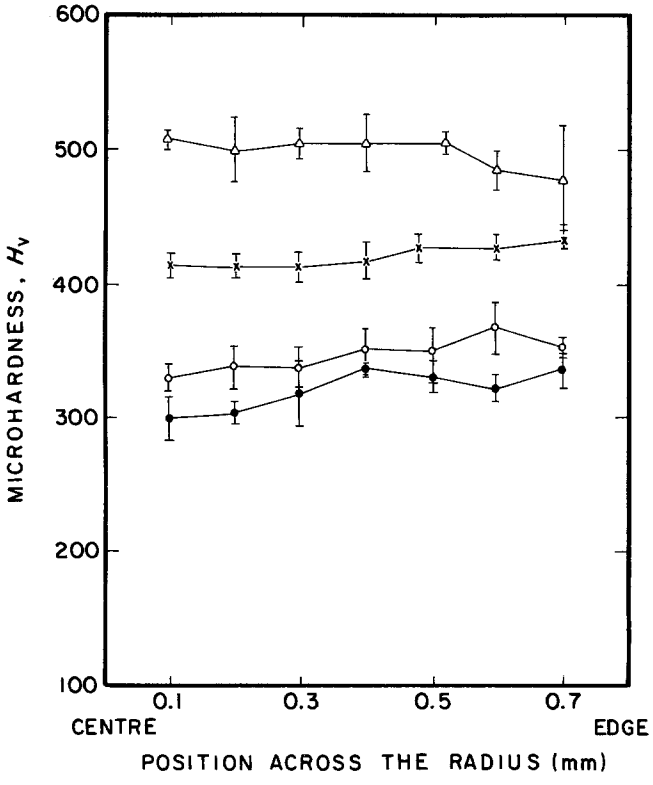

Figure 7 Variation of microhardness across the radius of the cross-section for selected samples of as-received IN 718 powder: (△) cold compaction, Test 33; (x) hot compaction and aged, Test 39; (○) hot compaction, 580° C, Test 38; (●) hot compaction, 740° C, Test 39.

strength. Selected samples were aged according to commercial ageing processes for Inconel 718 [19]. The yield strength in Test 43 increases from 877 to 1034 MPa, while the UTS increases from 1165 to 1210 MPa. Figs 9a and 9b show the nominal stress–strain curves for the specimens from tests 39 and 43, respectively, in the post-explosionem condition and after ageing. The yield strengths are much increased after ageing but the ductilities are decreased. Fracture followed yielding in aged samples. The added strength is evident, and one can clearly see the beneficial interaction between shock-hardening and thermal processing.

By comparing the yield strength and UTS of shock-consolidated and aged specimens to those of conventional wrought Inconel 718 aged at the same temperature, it is found that the shock-consolidated material does not have a higher tensile strength. The reported

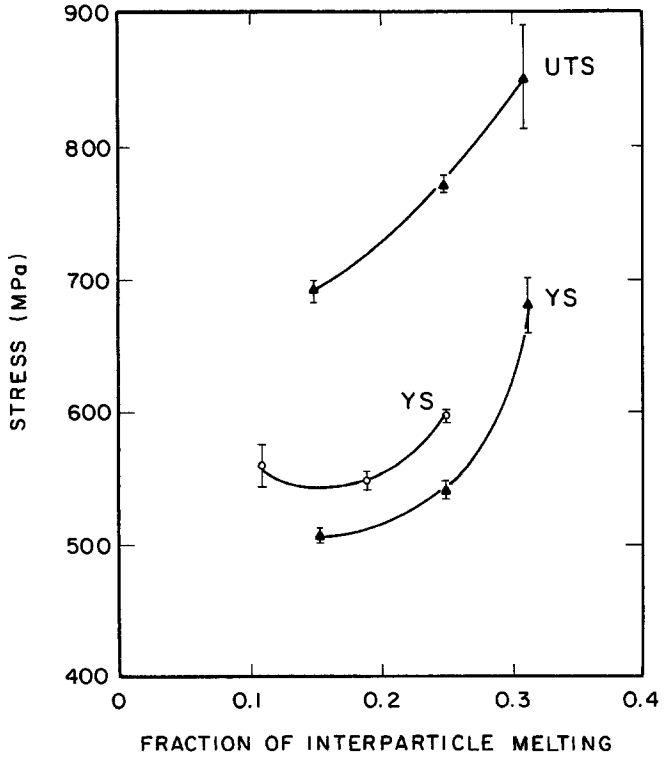

Figure 8 Variation of tensile strength with pre-heating temperature and interparticle melting: (○) 580° C pre-heated, (▲) 740° C pre-heated.

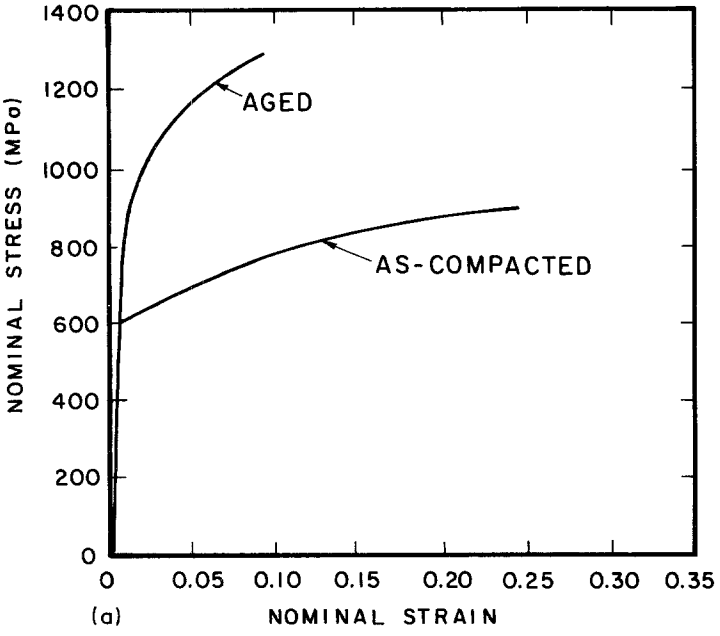

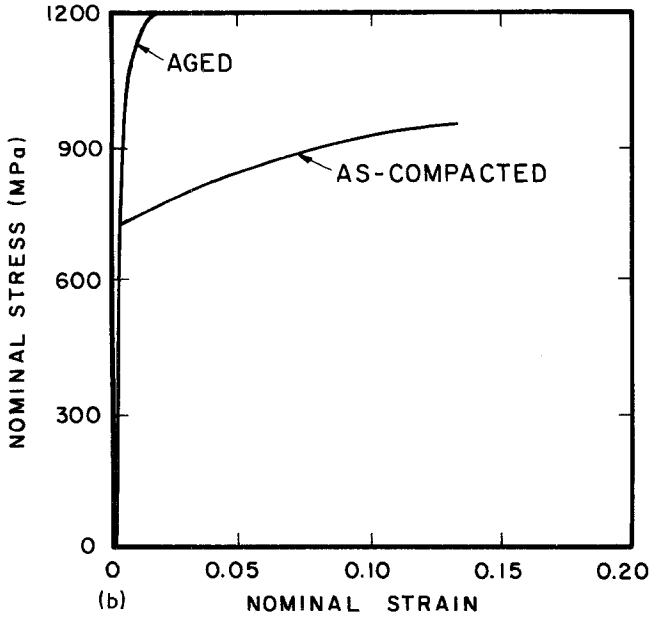

Figure 9 (a) Nominal stress–strain curve for Compact 39 in post-explosionem and aged conditions. (b) Nominal stress–strain curve for Compact 43 in post-explosionem and aged conditions.

yield strength and UTS values for wrought Inconel 718 thermally processed at 925° C/1 h/AC*, 720° C/8 h/FC* and 620° C/8 h/FC are 1056 and 1276 MPa, respectively. This behaviour may be due to the microvoids formed at interparticle melting zones in shocked material, as can be seen in the previous optical micrographs. These voids are believed to weaken the material. Another possibility is that the interparticle melting is not uniform around each particle. Poor bonding areas are weak points and are the starting points for interparticle fractures. These values are substantially lower than the strength obtained in compression for shock-consolidated Mar-M200 by Meyers and Pak [11]. Although Mar-M200 has a higher ambient-temperature strength, the large difference is attributed to (a) existing flaws causing a strength differential (compressive strength higher than tensile strength) and (b) substantial recovery and/or recrystallization for the hot-consolidation experiments.

The tensile strength of the specimens tested at General Electric is given in Table II. It can be seen that

TABLE II Tensile properties obtained at General Electric on 36 mm cylindrical specimens

Test No.	Test temperature (° C)	YS (MPa)	UTS (MPa)	Observations
26	R.T.	158	158	
	400	332	332*	
	650	22	26	
36	R.T.		802*	Broken in threads
	540		70	Broken in threads
38	R.T.		190	Broken in threads
	540		264*	

*AC = air cooled, FC = furnace cooled.

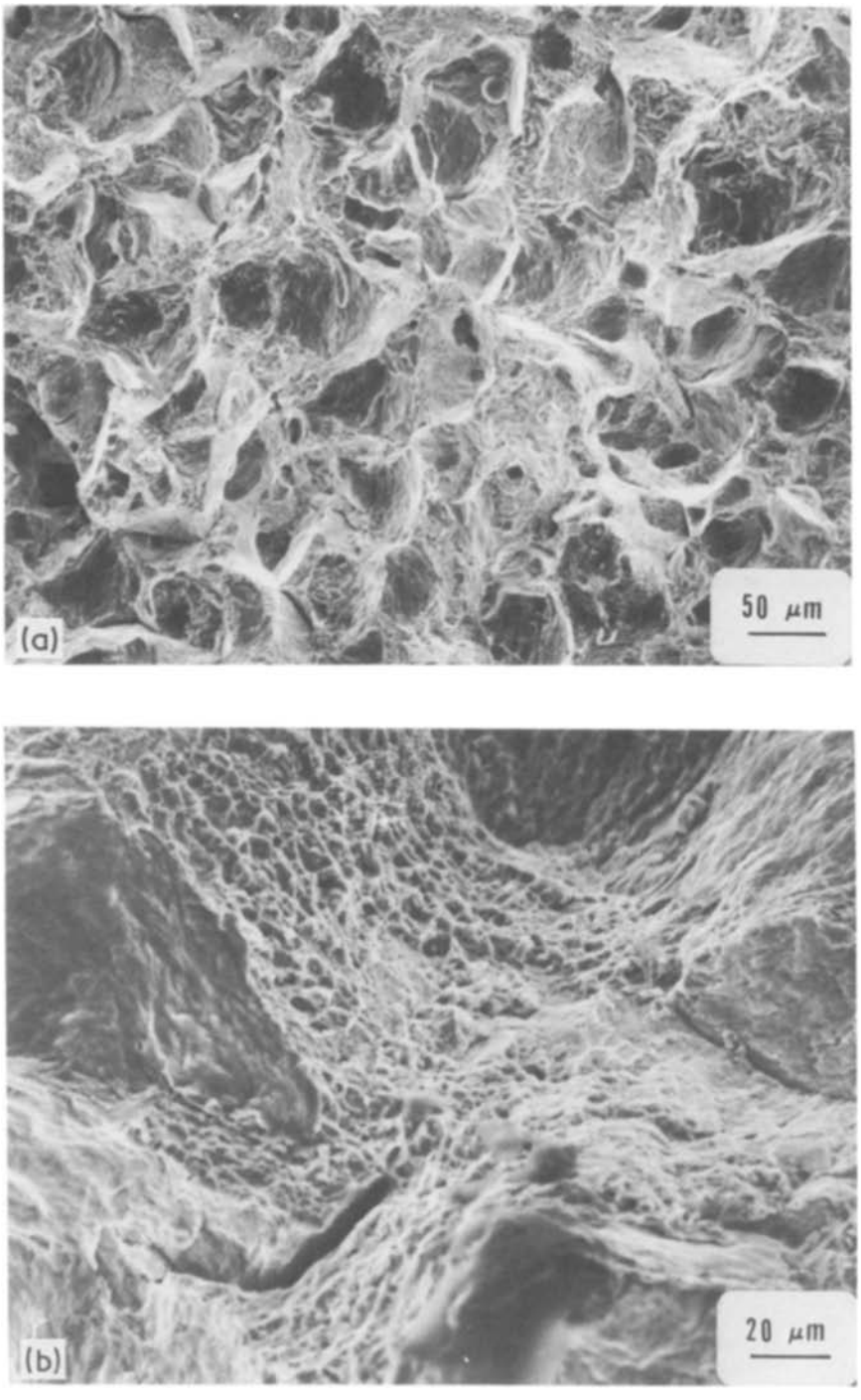

Figure 10 (a, b) SEM fractographs of failed tensile samples in double tube with big-gap compaction: (b) high magnification of (a).

there is no consistency between different tests. Some of these specimens fractured in the threads. The explanation for the variation in the tensile strength is the presence of microcracks. Actually, oxidized regions in the fracture surface were observed in the high-temperature tests, indicating pre-existing cracks. It seems that the three tests marked with asterisks reached the potential strength of the specimens. These strengths are of the same order than those wrought Iconel 718.

3.3.3. Fractography

The fracture surfaces of failed tensile specimens were observed by SEM. The fracture mode was predominantly interparticle rupture in single-tube (Test 31) and double-tube small-gap (Test 32) cold compacts. The particle surfaces in these specimens were heavily deformed, creating many facets. No evidence of melting due to shock compaction was present in these facets. Microvoids were present between the particles. Particles show mechanical interlocking with each other. Fractures can easily occur by pulling the particles away from an aggregate. The mechanical test revealed that these conditions had little (or no) mechanical strength.

The fractograph of the sample of the double-tube, big-gap, cold-compaction configuration (Test 33) presented a different fracture appearance, as shown in Fig. 10a. Two features were prevalent. Numerous particles were fractured by transparticle rupture. This indicates that when the interparticle bonding strength is higher than the particle strength, good consolidation between the particles can be expected. The typical fracture surface morphology observed in the

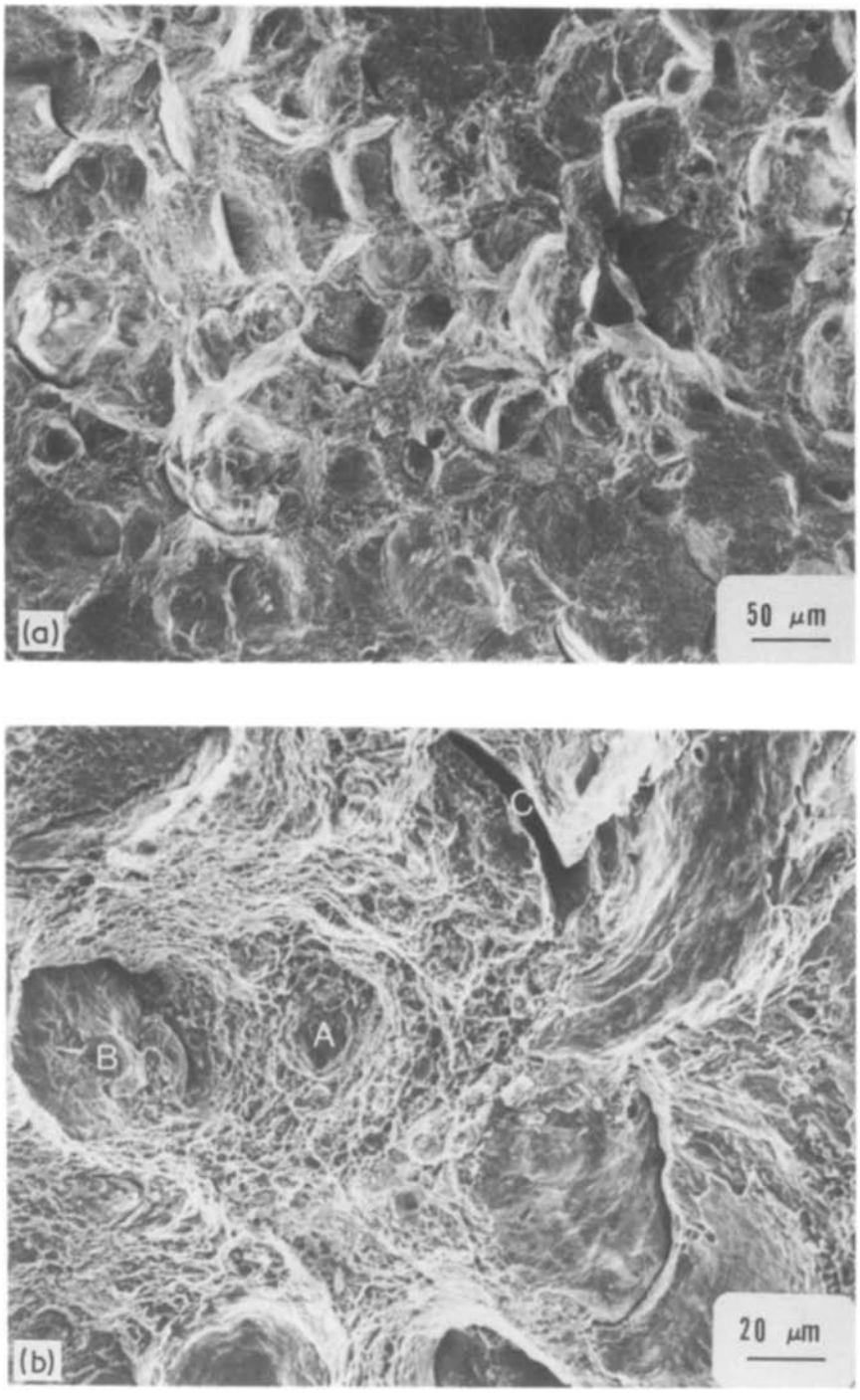

Figure 11 (a, b) SEM fractographs of failed tensile sample (Test 39) showing interparticle and transparticle fractures.

interparticle regions is the dimple structure, which is characteristic of the ductile fracture mode (see Fig. 10b). Voids and microcracks are also observed in the ductile regions. These defects are likely to be associated with crack initiation. The tensile stress–strain curve showed that this sample had considerable toughness.

A fractograph typical of specimens from pre-heated compacts is shown in Fig. 11. Tests 39 and 43 are both from specimens with high yield strength. Fractographs show a similar appearance to that of the cold compaction in Fig. 10, but transparticle failure seems to have increased. One can see in Fig. 11b that Point A is the dimple fracture initiation point, Point B is a fractured particle facet, and Point C is a microcrack.

3.3.4. Transmission electron microscopy of shock-consolidated powder

The microstructural modifications that occur within particles and particle boundaries, and that result from shock deformation and localized melting in shock-consolidated powders, were analysed. Both post-explosionem and aged conditions were examined. Generally, deformation twins, dislocation tangles and arrays, and deformation bands were formed in the interiors of the particles. The generation of deformation structures is strongly dependent on thermal and on mechanical histories, and on the stacking fault energy which is an intrinsic material property. Interparticle melt regions have been tentatively identified by Morris [4], Thadhani and Vreeland [13], and Meyers *et al.* [10], among others. Amorphous and

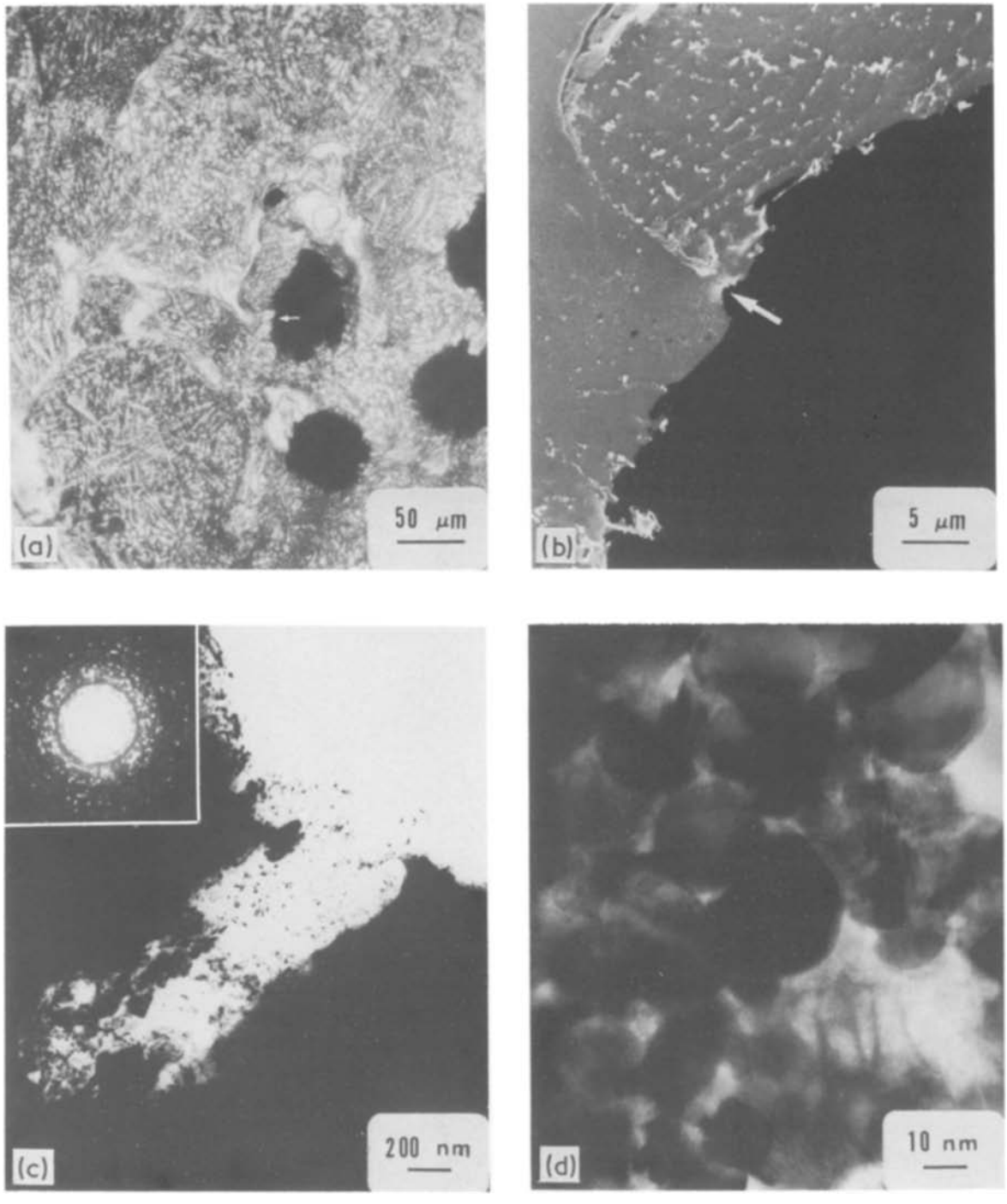

Figure 12 (a) Optical micrograph obtained by etching specimen used for transmission electron microscopy showing interparticle melt region (arrow); (b) scanning electron micrograph of the region pointed in (a); (c) transmission electron micrograph of the region pointed in (b) showing interparticle melting between two particles; (d) high magnification of interparticle melting region showing microcrystalline structure.

microcrystalline structures were observed in these regions, cooled at a high cooling rate.

An (apparent) interparticle melting region was examined using a specimen produced by double-tube big-gap cold compaction (Test 33). Fig. 12a shows an optical micrograph of the electron-transparent region (as arrow indicates) surrounding the electropolished hole in the thin foil specimen. Adjacent to the hole is a reasonably sized pool of white-etching material, as well as regions that exhibit the dendritic structure. Fig. 12b shows a scanning electron micrograph of the electron-transparent region indicated in Fig. 12a. Fig. 12c shows the interface between these regions by transmission electron microscopy. The particle boundary is completely eliminated due to melting, and the selected-area diffraction pattern shows that the interparticle melt regions can be described as microcrystalline. The fine dark phase in the interparticle melt region could be contamination from the original particle surfaces. Fig. 12d is a transmission electron micrograph of the interparticle melt region at a very high magnification, showing the extremely small sizes of the grains. This microcrystalline grain size is approximately 0.02 μm in diameter, corresponding to cooling rates of about 10^9 to 10^{10} K sec^{-1}. Moiré fringes are also observed in Fig. 12d, indicating that the micrographs are very close in orientation and some grains are overlapped.

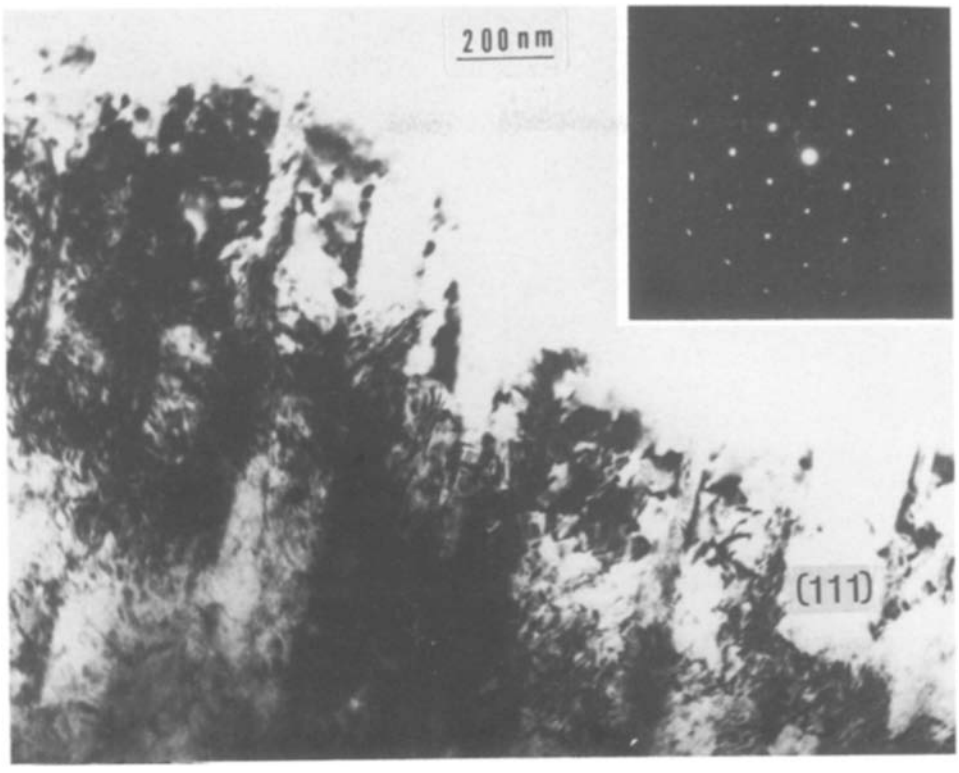

Figure 13 Defect substructure characteristic of particle interior.

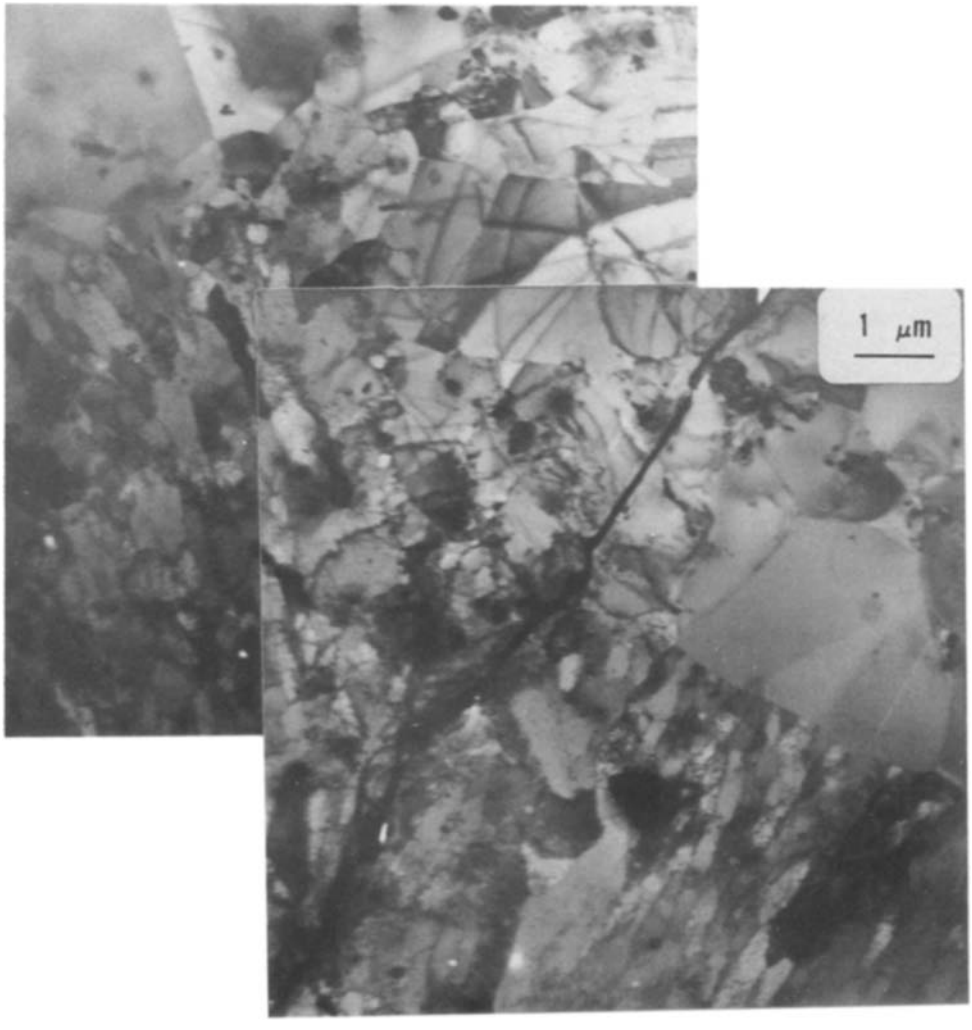

Figure 14 Transmission electron micrograph of compact pre-heated at 740° C (Test 39) showing recrystallization front separating deformation substructure consisting of cells and subgrains from annealed (dislocation-free) structure.

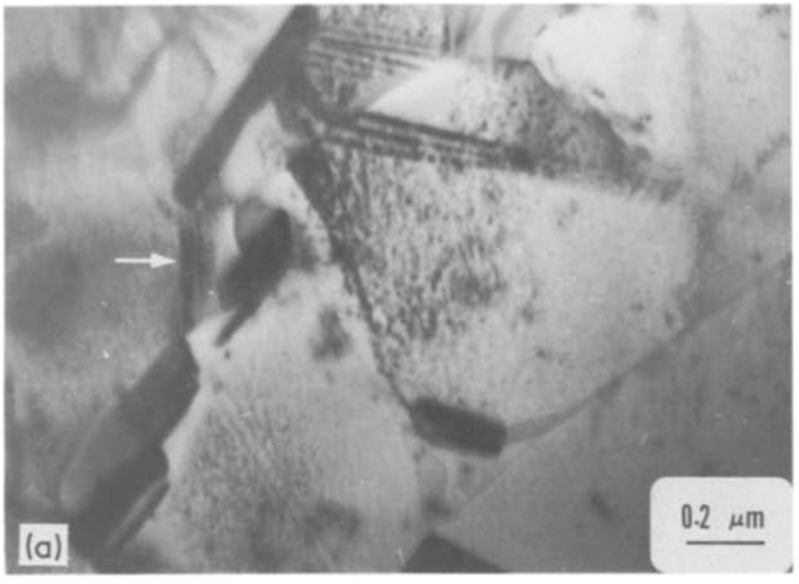

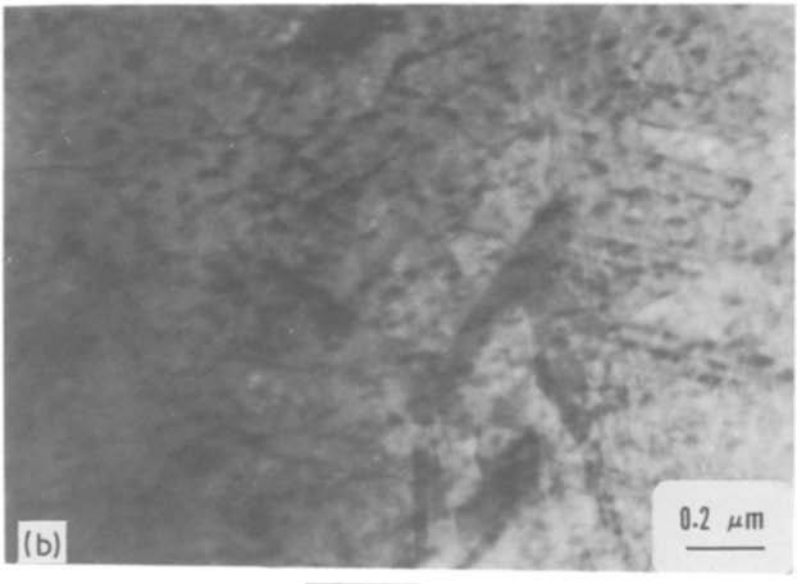

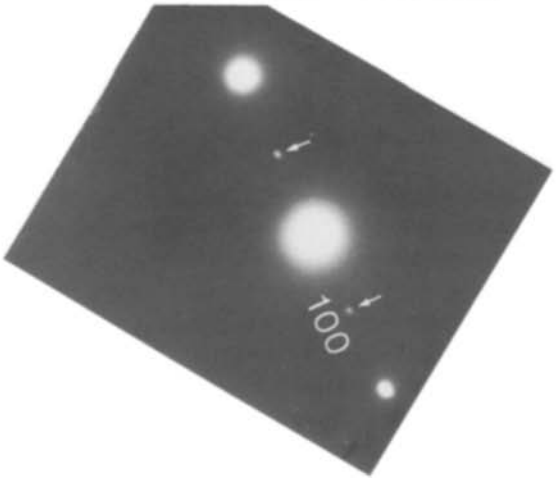

Figure 15 (a) Transmission electron micrograph of compact pre-heated at 525° C and aged (Test 43) showing grain-boundary precipitates. (b) Transmission electron micrograph of compact pre-heated at 525° C and aged (Test 43); γ'' precipitates evident from mottled appearance.

On the other hand, the banded substructure observed from the etched region which represents the inside of the particles is shown in Fig. 13. Deformation substructures typical of medium and low stacking-fault energy fcc alloys are exhibited. These bands seem to contain a very high dislocation density. The diffraction pattern of Fig. 13a shows that the banded structures are in quite different orientations. This is consistent with the interior of particles observed by Meyers *et al.* [10].

Compacts from Tests 39 and 43, which were warm-consolidated, were also selected for TEM examination. Fig. 14 shows the microstructures of specimens from Test 39 in the post-explosionem condition. In Fig. 14,

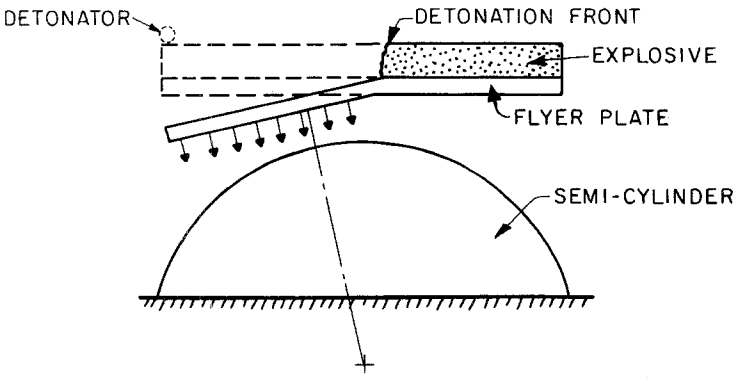

Figure 16 Schematic diagram of experiment in which flat plate is explosively accelerated on cylinder.

two distinct regions are seen in addition to a crack that might have been introduced in specimen preparation. Material at the lower side is found to be heavily deformed and partially recovered. Two large grains containing annealing twins and virtually dislocation-free are located in the upper part of the micrograph. These grains could be formed by recrystallization occurring immediately after the deformation. Precipitates also formed either in heavily deformed regions or in annealed regions. Precipitation is also possible during the pre-heating period before compaction. These precipitates were not identified, but are thought to be carbides. Annealing twins grow from the grain boundary toward the centre. Dash and Brown [20] proposed a mechanism for their formation, under grain-boundary migration conditions. Below the recrystallization front, there is a structure characterized by dislocation cells and subgrains; Gil Sevillano *et al.* [21] reviewed deformation substructures at high strains and described the transition from dislocation cells to subgrains at higher strains. Cells and subgrains are differentiated by the angle of misorientation. When the misorientation between cells reaches a certain critical level, subgrains are formed. It is thought that the heavy deformation introduced by shock consolidation is dynamically recovered, forming cells and subgrains.

Transmission electron microscopy of aged conditions revealed the expected change in substructure. Fig. 15a shows a micrograph of the specimen in Test 43 after ageing in a typical commercial two-stage treatment; the total ageing time was about 18 h. Full recrystallization was achieved in this specimen. Large precipitates (allotriomorphs) were formed at and aligned with the grain boundaries. These precipitates could be a δ-phase or a carbide. They are indicated by an arrow. Inconel 718 is a γ'' strengthened superalloy. γ'' has composition Ni_3Nb and has the b c t structure. It is coherent with the matrix. Fig. 15b shows the γ' or γ'' precipitates very clearly; the γ' precipitates were identified by the characteristic superlattice reflection in the diffraction pattern. Precipitates of γ' and γ'' can coexist in the Inconel 718 alloy [22]. The absence of massive γ' precipitates was predominantly due to the ageing time not being long enough. The size of γ' precipitates is also strongly dependent on the ageing temperature. Kear *et al.* [23] and Quist *et al.* [24] over-aged Mar M-200 and Inconel 718 as long as 60 h, and found that γ' or γ'' are of cuboidal shape. Cozar and Pineau [25] also over-aged Inconel 718 and found that the microstructure of the precipitates was identified as cube-shaped γ' particles coated with a γ'' shell over six faces. This morphology of precipitates has proved to have a very slow rate of coarsening.

3.4. Mechanism of shock consolidation

The mechanisms of shock consolidation have been discussed at length in the literature and the contributions of Raybould [2, 3], Morris [4, 5], Gourdin [6, 7], and Vreeland, Ahrens and co-workers [8, 9] comprise the main body of work. Recently, Williamson and Berry [26] simulated the deformation processing using the two-dimensional CSQ code and obtained a remarkable similarity in the particle deformation pattern with that observed by Morris [5] and Gourdin [27]. During the passage of the shock wave, the particles are violently thrust against each other. Morris [5] cited frictional sliding, explosive bonding, jet trapping and point deformation as the processes responsible for bonding. These processes cause intense heating at the particle surfaces and breaking of the oxide layers, which result in localized bonding. With the objective of better understanding the process of bonding, a model experiment was conducted. In the powder assembly spheres are thrust upon spheres, and the processes described above produce bonding. The model experiment utilized a flat plate thrust upon a semi-cylinder, for simplicity. Fig. 16 shows a schematic diagram of the assembly used (copper plate and semi-cylinder). The flat plate was accelerated downwards by an explosive (ANFO), initiated at one end. The impact of the plate on the semi-cylinder occurred at varying angles. At the initial contact of the plate (marked by dash-dotted line in Fig. 16) the impact is normal. As the sides of the plate progress downwards, the impact angle continuously increases. The resultant morphologies of the interface regions are shown in Fig. 17. The region where impact was normal did not exhibit bonding (central photograph in Fig. 17). It is well known in explosive welding technology that the impact angle between the two plates has to have a specific value. Plane parallel impact does not produce jetting. The two side photographs of Fig. 17 show the characteristic wave pattern of welded interfaces. This model experiment demonstrates that the contact points between the powder particles will not bond well. The inclined impact between powder surfaces, generating high localized deformation and, often, melting and jetting, is the process responsible for bonding. Thus, even well-consolidated powders have regions which should not be well consolidated. This is

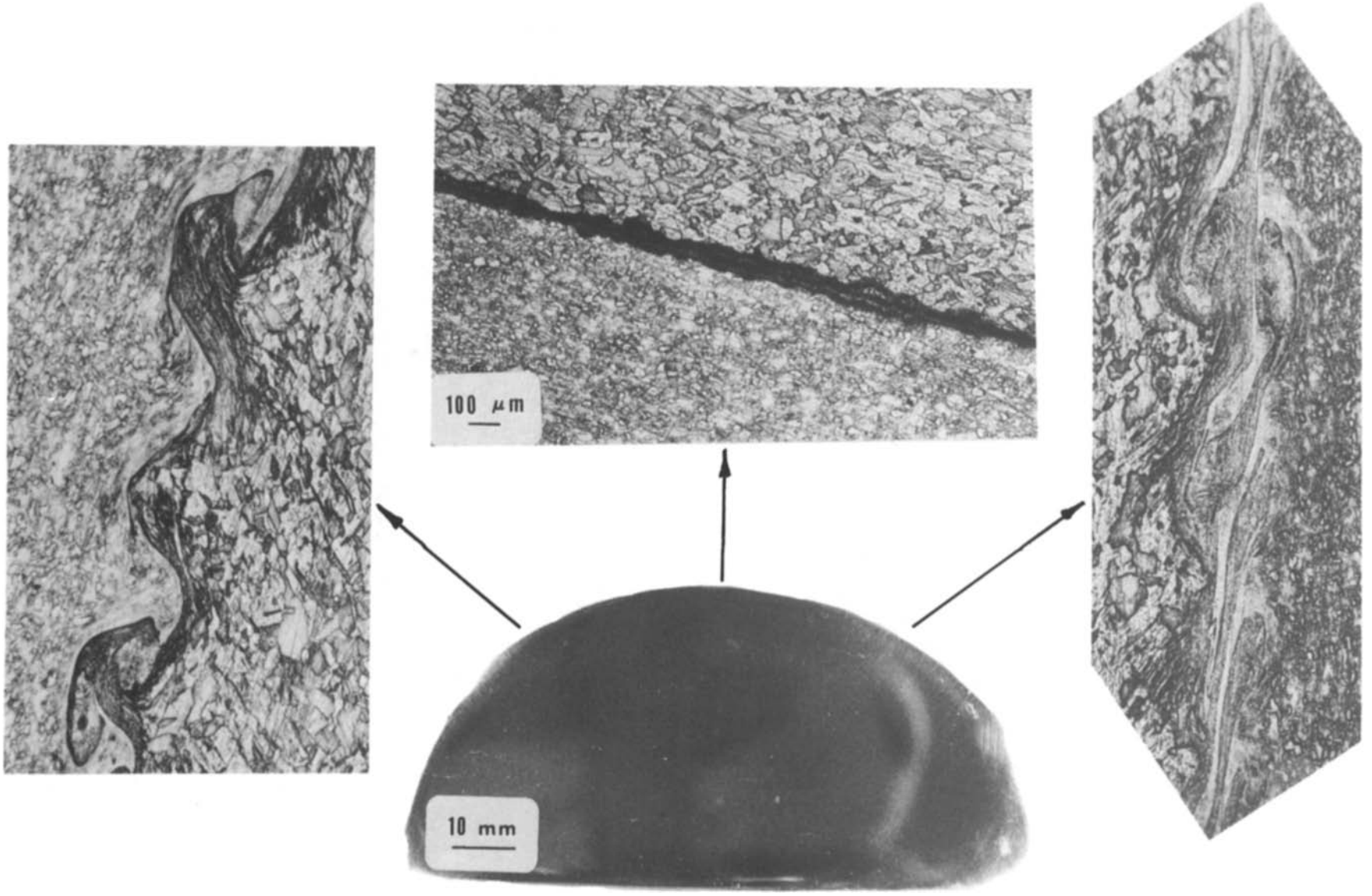

Figure 17 Metallographs of impact test in plate against semi-cylinder geometry.

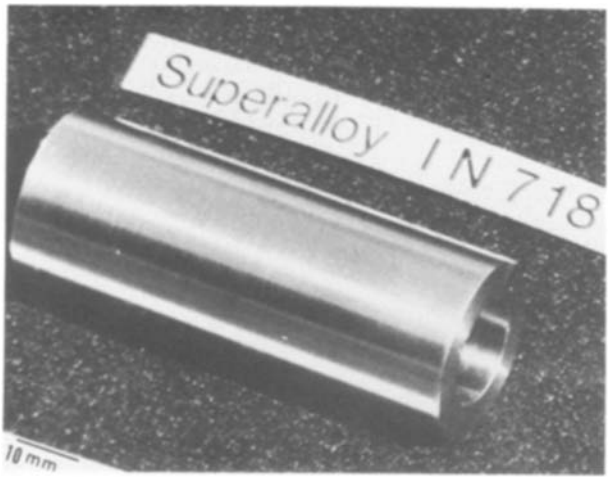

Figure 18 Photograph of specimen (Test 39) consolidated using double-tube big gap and pre-heating.

consistent with observations made on fracture surfaces. Even the best compacts had regions with interparticle fracture (evidence of poor bonding).

4. Summary and conclusions

It was demonstrated that 2.5 cm dia. × 10 cm length cylinders of IN 719 can be produced by shock consolidation of powder (Fig. 18). These cylinders have reasonable tensile properties but are not totally crack-free. The existence of microflaws is responsible for the dependence of tensile properties on the size of the specimen. Hence, subsequent mechanical processing would be required to eliminate existing imperfections. A parallel study [17] revealed that the process of explosive consolidation using the flyer-plate technique can be scaled up. Best consolidation is achieved by using a double-tube geometry with pre-heating of the compacts. Pre-heating tends to decrease cracking in the compacts. Shock consolidation at an initial peak pressure of 24 GPa and compact temperature of 525° C yielded the best tensile properties, with approximately 20% apparent interparticle melting and a yield stress of approximately 900 MPa. Transmission electron microscopy of specimens compacted at room temperature shows that the apparent interparticle melting region has a microcrystalline structure (grain size approximately 0.02 μm) and the particle interiors show a banded defect structure. Transmission electron micrographs of pre-heated compacts reveal the microstructure to consist of deformed regions with subgrains, microcrystalline, and annealed regions. A recrystallization front was observed; it separates the subgrain region from the annealed region. Micrographs of aged samples show a change to fully recovered and recrystallized microstructures. Massive precipitates appear at grain boundaries. These precipitates probably are a δ-phase or a carbide. Profuse small precipitates (20 nm in size) are distributed in the samples. It is strongly suggested that they are γ' and γ''.

Scanning electron microscopy fractographs show that fracture is of the interparticle rupture mode for those specimens with poor consolidation, and a mixture of interparticle and transparticle rupture mode for specimens with good consolidation. A ductile fracture is found in interparticle melting zones, and gives the consolidates a considerable toughness.

Acknowledgements

This research programme was financed initially by the National Science Foundation through Grant DMR 8115217, and later by the Center for Explosives Technology Research and by General Electric Aircraft Turbine Division. Dr R. Graham performed the seven calibrated experiments which provide a quantitative appraisal of the stress and temperature histories required for consolidation. Mr Dennis Hunter (TERA) directed the shock consolidation experiments and Dr A. Szecket conducted the ball-impact experiment. The TERA machine shop, managed by Mr K. Dillard, provided the essential support. The members of Mr Wang's thesis committee, Drs K. Staudhammer and A. Romig, provided valuable input through criticism. Dr P.-A. Persson, Director of CETR, and Mr A. Johnson, Manager for Advanced Materials and Processes, GE Aircraft Turbine Division, provided funding for a major portion of this programme. The tensile tests on the large specimens were conducted by Mr Paul Stanek, GE Aircraft Turbine Division.

References

1. "Dynamic Compaction of Metal and Ceramic Powders", NMAB-394 (National Materials Advisory Board, Washington, D.C., 1983).
2. D. RAYBOULD, *Int. J. Powder Met. Powder Tech.* **16** (1980) 9.
3. *Idem*, in "Shock Waves and High-Strain-Rate Phenomena in Metals", edited by M. A. Meyers and L. E. Murr (Plenum, New York, 1981) pp. 895–911.
4. D. G. MORRIS, *Metal Sci.* **16** (1982) 457.
5. *Idem*, *Mater. Sci. Eng.* **57** (1983) 187.
6. W. H. GOURDIN, *J. Appl. Phys.* **55** (1984) 172.
7. *Idem*, *Met. Trans.* **15A** (1984) 1653.
8. R. B. SCHWARZ, P. KASIRAJ, T. VREELAND Jr and T. J. AHRENS, *Acta Metall.* **32** (1984) 1235.
9. P. KASIRAJ, T. VREELAND Jr, R. B. SCHWARZ and T. J. AHRENS, *ibid.* **32** (1984) 1235.
10. M. A. MEYERS, B. B. GUPTA and L. E. MURR, *J. Metals* **33** (1981) 21.
11. M. A. MEYERS and H.-R. PAK, *J. Mater. Sci.* **20** (1985) 2133.
12. S. L. WANG, M. A. MEYERS and R. A. GRAHAM, in "Shock Waves in Condensed Matter", edited by Y. M. Gupta, (Plenum, New York, 1986) p. 731.
13. N. N. THADHANI and T. VREELAND Jr, *Acta Metall.* 34 (1986) 2323.
14. T. VREELAND Jr, P. KASIRAJ, A. H. MUTZ and N. N. THADHANI, in "Metallurgical Applications of Shock-Wave and High-Strain-Rate Phenomena', edited by L. E. Murr, K. P. Staudhammer and M. A. Meyers (Dekker, New York, 1986) pp. 247–276.
15. R. PRUMMER, in Proceedings of 4th International Conference on HERF, Estes Park, Colorado, 1973 (University of Denver, Denver Research Institute).
16. S. L. WANG, PhD thesis, New Mexico Institute of Mining and Technology, (1986).
17. M. A. MEYERS and S. L. WANG, *Acta Metall.* (1988) in press.
18. V. D. LINSE, in "Innovations in Materials Processing", edited by G. Bruggeman and V. Weiss (Plenum, New York, 1985) p. 381.
19. D. R. MUZYKA and G. N. MANIAR, in "Materials for Elevated Temperature Applications" (American Society for Metals, Metals Park, Ohio, 1979) p. 260.

20. S. DASH and N. BROWN, *Acta Metall.* **11** (1963) 1067.
21. J. GIL SEVILLANO, P. VAN HOUTTE and E. ADERNOUDT, *Prog. Mater. Sci.* **25** (1980) 69.
22. D. F. PAULONIS, J. M. OBLAK and D. S. DUVALL, *Trans. ASM* **62** (1969) 611.
23. B. H. KEAR, J. M. OBLAK and W. A. OWCZARSKI, *J. Metals* **6** (1972) 25.
24. W. E. QUIST, R. TAGGART and D. H. POLONIS, *Met. Trans.* **2A** (1971) 825.
25. R. COZAR and A. PINEAU, *ibid.* **4A** (1973) 47.
26. R. L. WILLIAMSON and R. A. BERRY, in "Shock Waves in Condensed Matter", edited by Y. M. Gupta (Plenum, New York, 1986) p. 341.
27. W. H. GOURDIN, *Mater. Sci. Eng.* **67** (1984) 179.

Received 19 May
and accepted 22 July 1987